Sigma J Eng Nat Sci, Vol. 43, No. 5, pp. 1473–1483, October, 2025

Sigma Journal of Engineering and Natural Sciences
Web page info: https://sigma.yildiz.edu.tr
DOI: 10.14744/sigma.2024.00153

Research Article

Broken rotor bar fault detection in induction motors through power spectral density to image method

Hatice OKUMUS[1,*], Ebru ERGUN[2]

[1]*Department of Electrical and Electronics Engineering, Karadeniz Technical University,Trabzon, 61080, Türkiye*
[2]*Department of Electrical and Electronics Engineering, Recep Tayyip Erdogan University, Rize, 53100, Türkiye*

ARTICLE INFO

Article history
Received: 09 May 2024
Revised: 18 July 2024
Accepted: 04 October 2024

Keywords:
Broken Rotor Bars; Deep Feature Extraction; Fault Diagnosis; Induction Motors; Machine Learning

ABSTRACT

Induction motors play an important role in a variety of industrial applications but are particularly sensitive to electrical faults, such as rotor-related problems such as broken rotor bars. Eliminating such faults is critical to reducing maintenance costs and preventing serious financial losses. This study presents a method based on detailed feature extraction for identifying broken rotor pull-out faults in induction motors. The process is initiated by generating spectrograms from sensor-based signals. However, instead of using these spectrograms directly, the resulting power spectral density data is converted into an optimized image format suitable for processing by pre-classified deep neural networks. To utilize these networks' capabilities, the developed features are fed into nearest neighbor (k-NN) and random forest classifiers for fault detection. The programmatic method was tested on a publicly available dataset of a three-phase step-down motor operating under various load conditions. In particular, the DenseNet201 model's improved features from the mean pooling structure yielded a remarkable accuracy of 99.75% using the random forest classifier. This result demonstrates a powerful and sensitive fault detection tool in induction motors by effectively integrating the conventional circuit techniques with detailed extraction by the proposed method.

Cite this article as: Okumus H, Ergun E. Broken rotor bar fault detection in induction motors through power spectral density to image method. Sigma J Eng Nat Sci 2025;43(4):1473–1483.

INTRODUCTION

Induction motors (IMs) are critical components in industrial environments thanks to their fundamental role in converting electrical energy into mechanical energy and are known for their high efficiency and robustness [1]. However, during operation these motors are subjected to constantly changing stresses such as radial and rotary electromagnetic forces and thermal distortion. These stresses can lead to various structural failures within the engine. Stator problems are often caused by the weakening of the insulation around the copper windings that can cause electrical short circuits. Rotor failures can occur for several basic reasons. Electrical problems such as overcurrent and electrical discharges can cause rotor bars to overheat and damage. Mechanical stresses such as vibration and misalignment can lead to cracks, while material defects in rotor components can lead to structural weakening. Additionally,

***Corresponding author.**
*E-mail address: haticeokumus@ktu.edu.tr

This paper was recommended for publication in revised form by Editor-in-Chief Ahmet Selim Dalkilic

thermal factors such as overheating and insufficient cooling cause thermal cycles that lead to wear on rotor materials [2]. Among rotor-related problems, broken rotor bar (BRB) failures are particularly common. These faults can seriously affect engine performance, causing increased vibration, decreased efficiency, overheating and electrical instabilities. Such disturbances can cause unpredictable torque output, which creates significant problems, especially in applications requiring precise control. Furthermore, BRB faults can increase maintenance and repair costs, increase the risk of motor failure, increase spare parts costs, and lead to operational downtime. Therefore, early detection and regular maintenance of these problems are crucial to maintaining the efficiency and lifespan of IMs.

Among BRB fault detection methods, Motor Current Signature Analysis (MCSA) can non-invasively identify faults by analyzing harmonic changes in the current's frequency [3,4]; vibration analysis reveals mechanical defects by evaluating the motor's abnormal vibration patterns[5]; thermal imaging detects overheating areas, visualizing problematic regions[6-8]; and frequency analysis detects faults through changes in operating frequency[2].

With the advancement of technology, tools such as artificial intelligence (AI) [9-11], machine learning (ML) [12,13], and advanced signal processing techniques [14,15] have been incorporated into broken rotor bar (BRB) fault detection methods. By leveraging big data analysis, AI and ML offer the opportunity to identify and predict faults by detecting abnormal behaviors based on data obtained from various sensors such as motor current, vibration, and temperature. Advanced signal processing techniques such as wavelet transform [16] and Fourier transform [17] enable more precise fault detection by revealing details and patterns in motor signals. In light of these advancements, several studies have introduced different methodologies for BRB detection and classification. Lizarraga-Morales et al. have developed an approach based on homogeneity as an index. The approach analyzes one phase of the induction motor startup-transient current, leveraging the homogeneity calculation. The arthurs also develope a hardware-processing unit based on a field programmable gate array device for online BRB detection and classification. The results demonstrate an accuracy greater than 99.7% for half, one, or two BRBs [18]. Chisedzi et al. have used decision tree classification, deep learning and artificial neural network methods for detecting BRB faults. Arthurs describe the process of identifying the faults by transforming the measured line-current signatures from time domain to frequency domain using discrete Fourier Transform. The decision tree method shows higher accuracy rates of 95% and 98% for 3BRB and 6BRB conditions [19]. Rayyam et al. have presented an approach using a combination of an ant lion optimizer (ALO) and an unscented Kalman filter (UKF) for broken bar fault monitoring in squirrel-cage induction motors (SCIM). The developed ALO-UKF algorithm adjusts the noise matrices for accurate fault detection. Simulation results showed better performance in broken bar detection compared to traditional methods such as the simple-UKF and EKF algorithms [20]. Ullah et al. carried out a study on fault detection and classification in induction motors using ANSYS Maxwell based simulations. Considering various loading conditions, stator current and leakage flux data were produced in normal and faulty cases (broken bar faults, full pole gap, static eccentricity). A deep neural network (DNN) algorithm was proposed and compared with support vector machines (SVM) and random forest classifiers (RFC) for fault detection and classification. Especially under 100% loading conditions, the DNN algorithm provided higher accuracy with leakage flux data compared to SVM and RFC. However, its performance was not as effective with stator current data [21]. Lee et al. proposed the combination of symmetric uncertainty (SU) and genetic algorithm (GA) to improve feature selection in induction motor fault classification. The SU-GA method was applied to four different engine cases and analyzed with the Hilbert-Huang transform (HHT). SVM classification was performed using SU, GA and SU-GA methods, and the SU-GA method achieved higher accuracy with fewer features. Additionally, simulations with varying levels of white noise confirm the effectiveness of the proposed method in classifying motor faults [22]. A feature fusion residual CNN with a double branch (DBF-CNN) for BRBs in IMs is proposed in [23]. This network utilizes the Hilbert transform to highlight fault features and employs a residual structure to prevent degradation. Furthermore, a double-branch structure extracts global and local features separately, while an attention-based feature fusion method addresses feature loss. Each of these studies contributes to the field of BRB fault detection and highlights the importance of combining traditional diagnostic methods with advanced technological advancements to increase the reliability and efficiency of IMs.

In the field of signal processing, utilizing advances in image analysis by converting signals into visual formats and enhancing their interpretive capabilities is attracting increasing interest. This technique combines the fundamental principles of signal processing with the advanced analytical power of image analysis. Numerous studies in the literature present this approach, encompassing different methods and applications. Some studies that explain this concept are summarized below.

Barrera-Llanga et al. proposed a Convolutional Neural Network (CNN) to detect broken rotor bars in squirrel-cage rotors. Using the Finite Element Method Magnetics (FEMM) software, they converted the current–angular position signals of a 28-bar squirrel-cage rotor into images and generated a dataset containing up to six broken bar scenarios at each location. Six different CNN architectures were evaluated in the study: Inception V4, NasNETMobile, ResNET152, SeNET154, VGG16, and VGG19. The VGG19 model performed best with an accuracy rate of

approximately 99% and achieved high precision, sensitivity and F1-score [24].

Shao et al. proposed a deep learning-based machine fault diagnosis method using time-frequency distributions obtained from wavelet transforms. In the study, the performance of the pre-trained models was compared with a CNN model trained from scratch on the same data. The proposed method was tested on three different datasets, and satisfactory results were obtained [25]. Huang and colleagues also detected machine faults using time-frequency distributions obtained from wavelet transforms. The Deep Continuous Convolutional Network (DCCN) uses multilayer perceptrons with Gaussian masks to parameterize continuous convolution kernels and multiplicative Gabor filters to increase noise resistance. Furthermore, depth-separated convolutions with residual connections are applied to increase computational efficiency. The effectiveness of DCCN has been validated using two laboratory datasets and one public dataset. The method achieved an average macro F1 score of over 98.69% in diagnosing various machine faults and an average score of 86.43% in a special test with reduced training data [26].

Our study also aims to detect BRB faults in electronic devices by adopting the principle of converting signals into visual representations. First, the signals collected from sensors on the electronic device are converted into spectrograms. However, instead of using these spectrograms directly, Power Spectral Density (PSD) data is converted into a visual format. Then pre-trained DNNs are used to extract features from these images. The resulting features are analyzed with k-Nearest Neighbor (k-NN) and Random Forest (RF) classifiers, to obtain accurate fault detection. The effectiveness of this technique has been validated using a dataset obtained from the University of São Paulo, Brazil, which includes normal and BRB fault conditions at four different severity levels and eight different load cases (from no load to full load). Among the 11 pre-trained DNN models, features extracted from the mean pooling layer of the DenseNet201 model, in particular, achieved an impressive accuracy rate of 99.75% when used with the RF classifier.

The remaining sections of this document is organized as follows: Section 2 details the proposed methodology and discusses the pre-trained DNNs along with the used classification techniques. Section 3 presents the performance evaluation. Section 4 concludes the study.

MATERIALS AND METHODS

The proposed method for detection of BRB faults is given in Figure 1. As indicated in the figure, vibration and current signals received from the sensors first undergo a preprocessing phase. During this preprocessing stage, the spectrogram of the signals is generated, followed by the conversion of the resulting PSD values into images. This preprocessing is executed independently for both the current and vibration signals. Following this, deep features are extracted from the resulting images using pre trained DNNs. The obtained features are combined and fed into RF and k-NN classifiers to assess their effectiveness.

PREPOCESSING

A spectrogram is a time–frequency representation that visualizes the evolution of a signal's frequency components over time [27]. It is obtained by applying the Short-Time Fourier Transform (STFT) to the signal *x(n)* which reveals how its frequency content changes with time. The STFT can be calculated as shown in Equation (1):

$$STFT\{x(n)\}(m,\omega) = \sum_{n=-\infty}^{\infty} x(n) \cdot w(n-m)\, e^{-j\omega n} \quad (1)$$

In this equation:

x(n) is the signal being analyzed.

w(n-m) represents the window function, centered at time m.

$e^{-j\omega n}$ is the complex exponential function, where ω denotes the angular frequency.

As previously mentioned, this study does not directly utilize the spectrograms of the signals. Instead, it focuses on the Power Spectral Density (PSD) values deriven from the spectrogram process. The PSD is obtained with Equation (2):

$$PSD = \frac{|STFT|^2}{N x f_s} \quad (2)$$

Where N denotes the sample length while f_s indicates the sampling frequency.

The PSD values obtained are converted into a logarithmic scale, *10*log10(PSD)*, significantly improving the visualization of the signal's time-frequency content.

Deep learning models typically require input data in a three-channel (RGB) image format. To meet this requirement, we converted our initial single-channel dataset to a three-channel format by concatenating it. This way, each channel contains the same information; while this may seem unnecessary, it is essential to comply with the model's structural input format requirements. This format simplifies the process of the usage of advanced pre-trained models without the need of specific retraining for single-channel input, allowing for the efficient use of existing deep learning architectures.

Feature Extraction

DNNs are deep learning models commonly used in tasks such as image recognition. Layers like convolutional, pooling, fully connected, and activation functions make up a typical DNN. The network needs more computational power as layers are added because there are more parameters to learn. While training models on larger datasets give better performance, this process can be time-consuming. Therefore, transfer learning has become widespread. Transfer learning allows pre-trained models to

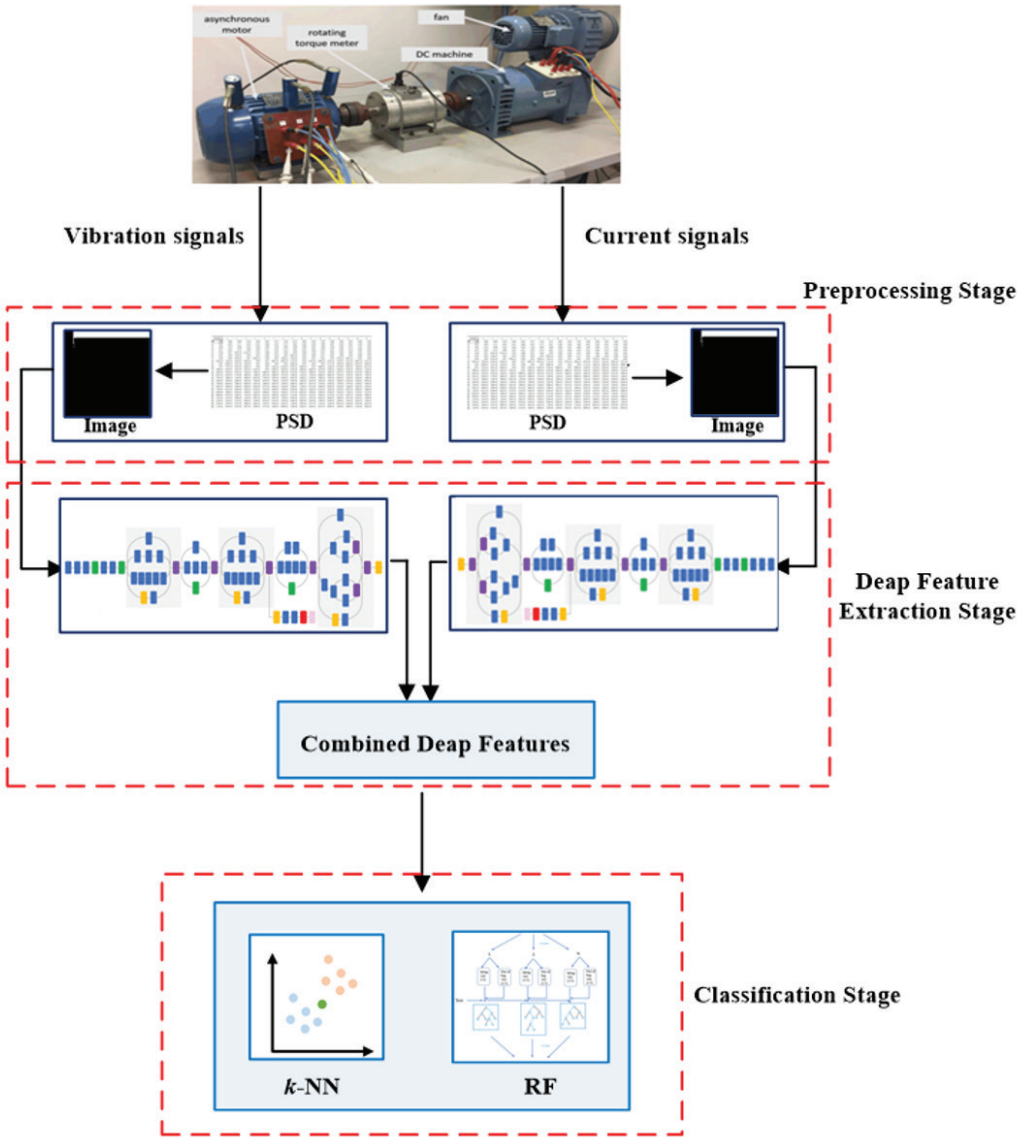

Figure 1. Block diagram of the proposed method.

be reused for different tasks. Furthermore, using knowledge from similar tasks can require less data than training from scratch. Many different DNN architectures have been developed over the years such as VGG, DenseNet, SqueezeNet, ResNet, MobileNet, AlexNet and Inception. In this study, 11 pre-trained models which are VGG-16, VGG-19, DenseNet-201, SqueezeNet, ResNet-50, MobileNetV2, AlexNet, Inception V3, NasNetMobile, DarkNet53, and Inception-ResNet-v2 are used for feature extraction.

The VGG-16 and VGG-19 models, created by the Visual Geometry Group (VGG) at the University of Oxford and first presented by Simonyan & Zisserman in 2014, are renowned for their structural simplicity and reliance on just three 3x3 convolutional layers [28]. The VGG-16 model has 16 layers (13 convolutions, 3 fully connected) while the VGG-19 model has 19 layers (16 convolutions, 3 fully connected). Although they have simple design both models performed well in the ImageNet Large Scale Visual Recognition Challenge (ILSVRC) and are now among the main reference models for image classification. The VGG models are widely used feature extractors in many applications, particularly in deep learning research, due to their simplicity and practicality.

With 201 levels, DenseNet-201 is an enhanced version of the DenseNet architecture [29]. When compared to other deep architectures, this model has demonstrated exceptional performance on common benchmarks such as the ImageNet dataset, effectively addressing the vanishing-gradient problem and yielding higher accuracy with more economical parameter usage.

Researchers at DeepScale, Stanford University, and the University of California, Berkeley developed SqueezeNet in

2016, which presents the novel idea of "fire modules" [30]. These modules, which are designed to compress (squeeze) input channels before expanding them, effectively replace conventional convolutional layers, significantly reducing the model's parameter count. As a result, a remarkably small network is produced, which is perfect for installation on devices with limited processing power or in embedded systems.

ResNet-50, a variant of the Residual Network (ResNet) designed by Kaiming He and his team at Microsoft Research, features a total of 50 layers (encompassing 177 sub-layers) [31]. ResNet broke the previous record in the 2015 ILSVRC competition with an error rate of just 3.37%. ResNet-50's depth and effectiveness have made it a popular model for a variety of computer vision applications, highlighting its importance in the field.

Introduced in 2018 by Google's research team [32], MobileNetV2 is a distinguished CNN architecture within the MobileNet series, designed to deliver models of high efficiency suitable for devices constrained by their computational power. Inverted residuals and linear bottleneck modules are integrated in this version, which advances from its predecessor, MobileNetV1. Distinct from conventional residual blocks that upscale dimensionality before convolution, MobileNetV2's innovative bottleneck approach initially compresses dimensionality, conducts convolution, and subsequently restores the dimensionality. This approach minimizes model dimensions and maximizes computing performance, making it very beneficial for mobile systems. Moreover, MobileNetV2 makes use of depthwise separable convolutions, which significantly reduce computational burden and parameter count by splitting a normal convolution into a depthwise convolution and a 1x1 pointwise convolution.

AlexNet is a deep learning architecture introduced by Krizhevsky, Sutskever, and Hinton [33] that significantly advanced developments in computer vision. AlexNet consists of eight main layers; five convolutional layers and three fully connected layers. When pooling, ReLU (Rectangular Linear Unit), normalization, and softmax layers are included, the total number of layers of the architecture reaches 25. Having 62 million trainable parameters, AlexNet is designed to process 227x227 images, highlighting its complexity and capacity in processing visual data. With 62 million trainable parameters, AlexNet is designed to process images of size 227x227, underscoring its complexity and capacity for handling intricate visual data.

Google's 48-layer deep, pre-trained convolutional neural network model, Inception V3 network, is an additional development in CNN utility [34]. It performed admirably in the ILSVRC-2015 competition, achieving a top-5 accuracy rate of 92.8%. The use of tiny convolution kernels rather than huge ones is one of Inception V3's primary architectural innovations. This is achieved by breaking down conventional bigger convolutions into a mix of one- and two-dimensional convolutions, i.e., into sequences of 1xN and then Nx1 convolutions. By using a strategic decomposition the model's parameter count is dramatically reduced, improving its efficiency without compromising performance.

The NasNetMobile, a creation of the Google Brain team unveiled in 2017, embodies a design rooted in neural architecture search (NAS) principles [35]. The regular cell and the reduction cell are two different kinds of building components used in this construction. Multiple layers in normal cells improve feature map resolution, allowing for more in-depth picture analysis. Reduction cells, on the other hand, reduce the amount of data to be processed by reducing the spatial resolution of feature maps, thus ensuring more efficient processing. The final design is built by carefully placing these components in the right order to maximize the neural network's depth and efficiency.

DarkNet53, an artificial intelligence model developed by Joseph Redmon, serves as the cornerstone of the YOLO (You Only Look Once) algorithm [36]. This model is widely used in deep learning and image processing fields, and shows high performance especially in real-time object detection applications. With the elements from the Deep Residual Network and DarkNet19 architectures, DarkNet53 is based on the sequential use of 1x1 and 3x3 convolutional layers with residual connections. This structure improves the model's ability to efficiently process and analyze visual data, enabling it to identify objects in images with high accuracy and speed.

The Inception-ResNet-v2 model which stands out for its 164-layer architecture expertly blends the advantages of the ResNet (Residual Networks) and Inception models [37]. The goal of this combination is to improve computer vision capabilities by combining ResNet's superiority in training very deep networks through residual connections with the Inception architecture's skill on processing multi-scale picture information. This model which is designed to process 229x229 pixel image inputs, consists of a complex hierarchy of convolutional, pooling and dense layers. The model's effectiveness in feature extraction and recognition is improved by this deliberate layering, which makes it a powerful tool for a variety of computer vision applications.

CLASSIFICATION METHODS

Random Forest (RF)

RF is a powerful technique that employs multiple decision trees to perform both classification and regression tasks [38]. It builds these trees by randomly sampling n datasets from the original training data using the bootstrap method. At each node of every tree, a subset of m variables is randomly selected, and the best split is determined based on the Gini index [39]. After choosing the optimal split, the tree is further divided into two branches. This process continues until each leaf node represents a single class [40]. The performance of each tree is evaluated by its Out-of-Bag

(OOB) errors, which are a measure of prediction accuracy on data not included in the bootstrap sample. Trees with lower OOB errors are considered more accurate and are given higher weight whereas those with higher errors receive lesser weight. When making predictions, each tree casts a vote weighted by its accuracy. The final classification decision is based on the majority of these weighted votes across all n trees, with the class garnering the most votes being declared the final outcome.

k- Nearest Neighbours (k-NN)

The k-Nearest Neighbors (k-NN) algorithm is a straightforward machine learning method widely used for classification and regression tasks such as image classificatio, power load forecasting, fault detection and medical diagnosis. In this approach, predictions for a given data point are determined based on the labels or values of its closest k neighbors. The algorithm typically identifies these neighbours using a distance metrics such as Euclidean, Manhattan and Minkowski Distance. In classification cases, the most frequent class label among these neighbours is returned as the output; in regression, it calculates the average of these neighbours output values. The effectiveness of this method heavily depends on the correct determination of the 'k' value.

In this study, the Euclidean distance metric is employed to compute the distances between neighbors. The calculation of Euclidean distance between two points, r and s, in an n-dimensional space is defined as shown in Equation (3) [41].

$$d_E(r,s) = \sqrt{\sum_{i=1}^{n}(r_i - s_i)^2} \tag{3}$$

RESULTS AND DISCUSSION

In this study, a dataset containing data from an induction motor with broken rotor bar faults, made publicly available by the University of São Paulo in Brazil, was used [42]. The data set includes a four-pole, three-phase motor with an output power of 1 hp, a supply voltage of 220/380V, and a nominal speed of 1785 rpm. Faults are divided into four levels (from 1 to 4) according to the number of broken rods, and a separate category is defined for fault-free engines (health class).

To comprehensively evaluate these categories, eight different load cases were determined, with torque values ranging from 0.5 Nm to 4.0 Nm, in 0.5 Nm increments. For each condition, 10 experiments were conducted to comprehensively collect both electrical and mechanical signals. The experimental setup for the dataset is shown in Figure 2.Some sample examples of the images transformed from PSD values for healthy and broken rotor bar under different load conditions are given in Figure 3.

Due to the varying sizes of each signal recorded from sensors, in this study, 1001000 data points are used for current signals (I_a), and 140000 data points for vibration signals (V_{ib_acpi}). As stated before there are 8 different loading conditions and 5 fault classes, and each experiment repeated 10 times, resulting in a total of 400 image data. This dataset is randomly split into 80-20% for training and testing. To ensure more stable and accurate results, this process is repeated 10 times.

The classification accuracy results for 11 different DNN models, showing the performance analysis at various layers using k-NN and RF methods, along with the standard deviations are given in Table 1 Among these architectures, DenseNet201 (avg_pool) and InceptionV3 (avg1) have given the highest performance with almost perfect accuracies of 99.75% and 99.25%, respectively, with the RF classifier. Meanwhile, InceptionResNetV2, NasNetMobile (global avgpooling2d), and AlexNet (fc8) achive lower accuracies of 78.25%, 80.62%, and 81.87%, respectively, when using the k-NN algorithm. These results show that most models perform better with RF compared to k-NN, suggesting that RF's model utilizes the deep features generated by these networks more effectively.

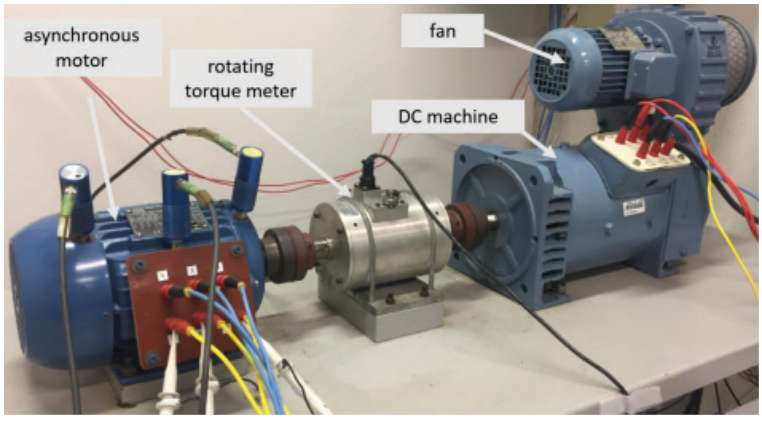

Figure 2. Experimental setup.

Table 1. Classification accuracy results using V_{ib} and I_a signals

Deap feature	*k*-NN	RF
AlexNet (fc7)	88.37±2.5	97.87±1.56
AlexNet (fc8)	81.87±4.80	96.75±2.14
DenseNet201 (avg_pool)	96±1.64	**99.75±0.53**
MobileNetV2 (global avg pooling2d)	93.62±2.32	99±0.79
DenseNet201 (fc1000)	95.5±1.21	97.62±1.09
InceptionV3 (avg_pool)	89.12±1.96	99.25±1.05
Vgg19 (fc7)	91.5±2.02	98.75±1.18
Vgg16 (fc7)	94.37±2.52	98.37±1.03
SqueezNet (pool10)	82.6±3.03	93.12±3.45
DarkNet53 (avg1)	98.50±1.64	98.75±1.56
NasNetMobile (global avg pooling2d)	80.62±3.50	96.12±2.08
Inception-ResNetV2 (avg_pool)	78.25±4.94	92.62±2.24
ResNet50 (fc1000)	89.75±3.67	98.62±1.37

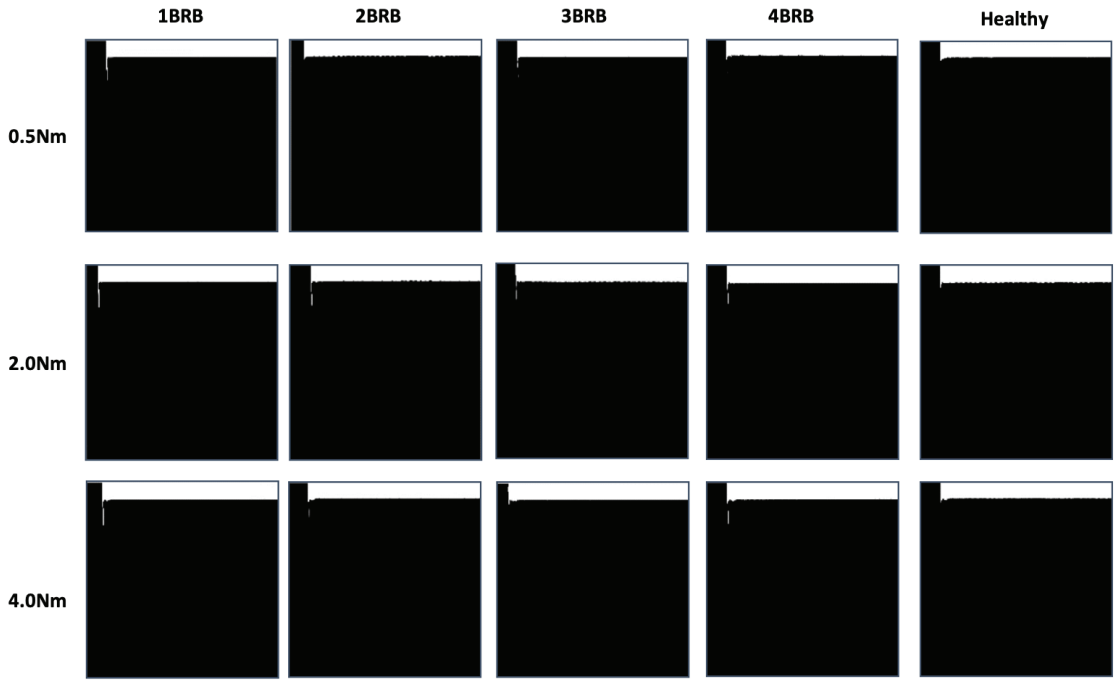

Figure 3. PSD-Image transformed samples for healthy and broken rotor bar under different load conditions.

If a closer look is taken at the standard deviation values as illustrated in Figure 4, it can be observed that the k-NN algorithm follows a trend ranging between 1.21 and 4.94, while the RF classifier exhibits standard deviation values between 0.79 and 3.45. These values clearly demonstrate that the RF classifier provides more consistent results in solving the BRB fault detection problem.

In the literature, there are studies that attempt BRB fault detection using only current data. Consequently, this study has also examined the impact of I_a current signals on fault detection results. When reviewing the results in Table 2, it is observed that classifications carried out using the *k*-NN method generally provide better outcomes compared when using the combined features. While for the RF method, the use of combined features are found to be more effective. The highest overall result is once again obtained using the DenseNet201 model (avg_pool) combined with RF classification. The standard deviation

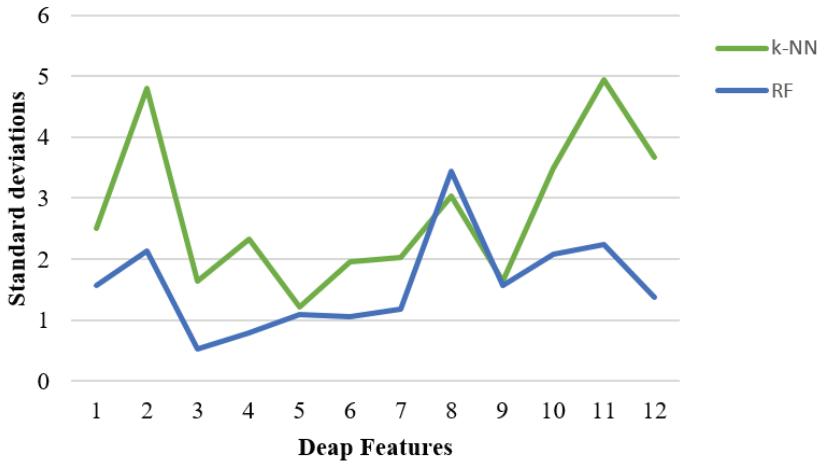

Figure 4. Standard deviation results.

results consistently demonstrate that the *k*-NN method is significantly more effective when extracting features solely from I_a signals.

The method introduced in this study is evaluated against previous research, as outlined in Table 3, all using the same dataset. References [43,44] and [45] implement a transformation of signals to images, with significant variations in approach. Whereas, reference [23] applies the Hilbert transformation to signals and feeds the transformed data into a dual-branch CNN model. In contrast to other studies in the comparison, reference [23] addresses a three-class problem involving 1BRB, 2BRB, and 3BRB and achieves an accuracy of 99.86%, whereas the others tackle a more complex five-class scenario, including HLT, 1BRB, 2BRB, 3BRB, and 4BRB. Moreover, both References [43] and [44] create spectrogram images from signals. However, the used methodologies are different; reference [44] uses only current signals and the short time fourier transform (STFT) for spectrogram generation, while reference [43] incorporates both vibration and current signals, employing the continuous wavelet transform (CWT) to produce spectrograms, this approach yields an accuracy score of 100%. Reference [44] takes a different approach by using time-domain grayscale current imaging techniques coupled with CNN, yielding a 99.53% accuracy.

The proposed methods in this study which employ PSD transformations to image format followed by deep feature extraction, exhibit an effective approach to the classification task. The first proposed model achieves an accuracy of 98.5% using current signals, while the second, utilizing both vibration and current signals, reaches 99.75% accuracy.

Table 2. Classification accuracy results using I_a signals

Deap Feature	*k*-NN	RF
AlexNet (fc7)	97.50±1.67	97.25±1.54
AlexNet (fc8)	96.37±1.24	96.12±1.71
DenseNet201 (avg_pool)	95.8±2.83	**98.5±1.15**
MobileNetV2 (global avg pooling2d)	93±2.84	94.6±3.44
DenseNet201 (fc1000)	93.5±2.55	96±3.05
InceptionV3 (avg_pool)	97.5±1.02	98.5±0.99
Vgg19 (fc7)	94.25±2.22	95.62±1.69
Vgg16 (fc7)	95.25±2.49	95.37±1.56
SqueezNet (pool10)	93.12±3.50	94.5±.71
DarkNet53 (avg1)	98. ±1.58	98.37±1.67
NasNetMobile (global avg pooling2d)	96.12±2.34	96.2±1.86
Inception-ResNetV2 (avg_pool)	97±1.79	96.12±1.50
ResNet50 (fc1000)	95±2.95	96.12±2.32

Table 3. Comparison with the research in the literature

Reference Study	Method	Used signal	Accuracy (%)
[23]	Hilbert transform+double-branch fusion residual CNN	Current signals	99.86
[43]	Spectogram images with CWT+deap features	V_{ib_acpi} and I_a	100
[44]	Spectogram images +CNN	Vibration signals	97.67
[45]	Time domain grayscale current imaging technique+ CNN	Current signals	99.53
Proposed	PSD to image transform+ Deap feature extraction	I_a	98.5
Proposed	PSD to image transform+ Deap feature extraction	V_{ib_acpi} and I_a	99.75

CONCLUSION

This study proposes a robust method for detecting BRB faults in IMs using advanced deep feature extraction techniques. By converting PSD data into image formats which can be analyzed by pre-trained DNNs, the proposed approach effectively utilizes different properties of motor signals. The use of k-NN and RF classifiers improves the fault detection process by enabling precise detection of faults that vary under different load conditions. Validation of this approach was performed with publicly available dataset provided the University of São Paulo, Brazil, containing normal and BRB fault cases at four different severity levels and eight different load scenarios. The DenseNet201 model achieved a high classification accuracy of 99.75% with its average pooling layer along with the RF classifier using both vibration and current signals. DenseNet201's densely connected architecture, parameter efficiency, and depth make it a powerful model. The average pooling layer improves performance by providing a comprehensive summary of features, providing robustness to noise, and encouraging balanced learning. These features allow DenseNet201 to outperform other models, making it particularly suitable for complex and sensitive tasks such as BRB fault detection. This research sets a benchmark for future studies aimed on fault detection in IMs. Creating a comprehensive dataset with different motor types, fault conditions and operating scenarios will be beneficial for further development. Also, the accuracy and robustness of fault detection can be greatly increased by using ensemble methods and real-time data processing.

AUTHORSHIP CONTRIBUTIONS

Authors equally contributed to this work.

DATA AVAILABILITY STATEMENT

The authors confirm that the data that supports the findings of this study are available within the article. Raw data that support the finding of this study are available from the corresponding author, upon reasonable request.

CONFLICT OF INTEREST

The author declared no potential conflicts of interest with respect to the research, authorship, and/or publication of this article.

ETHICS

There are no ethical issues with the publication of this manuscript.

STATEMENT ON THE USE OF ARTIFICIAL INTELLIGENCE

Artificial intelligence was not used in the preparation of the article.

REFERENCES

[1] Gündoğdu T. Torque capability comparison of induction and interior permanent magnet machines for traction applications. Gazi Univ J Sci 2023;1:1. [CrossRef]

[2] Kumar P, Hati AS. Review on machine learning algorithm based fault detection in induction motors. Arch Comput Methods Eng 2021;28:1929–1940. [CrossRef]

[3] Ince T, Kiranyaz S, Ren L, Askar M, Gabbouj M. Real-time motor fault detection by 1-D convolutional neural networks. IEEE Trans Ind Electron 2016;63:7067–7075. [CrossRef]

[4] de Las Morenas J, Moya-Fernandez F, Lopez-Gomez JA. The edge application of machine learning techniques for fault diagnosis in electrical machines. Sensors 2023;23:2649. [CrossRef]

[5] Delgado-Arredondo PA, Morinigo-Sotelo D, Osornio-Rios RA, Avina-Cervantes JG, Rostro-Gonzalez H, Romero-Troncoso RJ. Methodology for fault detection in induction motors via sound and vibration signals. Mech Syst Signal Process 2017;83:568–589. [CrossRef]

[6] Sasikumar B, Venkatasalam K, Rajendran P. Induction motor fault detection and classification using RCNN and SURF based machine learning algorithms and infrared thermography. Sci Iran 2024. doi: 10.24200/SCI.2024.61897.7589 [Epub ahead of print] [CrossRef]

[7] Resendiz-Ochoa E, Enriquez-Ugalde JM, Saucade-Dorantes JJ, Morales-Hernandez LA. Broken rotor bar failures diagnosis with supervised learning and infrared thermography. In: IEEE 13th International Symposium on Diagnostics for Electrical Machines, Power Electronics and Drives (SDEMPED). Dallas (TX): IEEE; 2017. p.499–504. [CrossRef]

[8] Trejo-Chavez O, Cruz-Albarran IA, Resendiz-Ochoa E, Salinas-Aguilar A, Morales-Hernandez LA, Basurto-Hurtado JA, et al. A CNN-based methodology for identifying mechanical faults in induction motors using thermography. Machines 2023;11:752. [CrossRef]

[9] Elhaija WA, Al-Haija QA. A novel dataset and light-weight detection system for broken bars induction motors using optimizable neural networks. Intell Syst Appl 2023;17:200167. [CrossRef]

[10] Khishe M. Variable-length CNNs evolved by digitized chimp optimization algorithm for deep learning applications. Multimed Tools Appl 2024;83:2589–2607. [CrossRef]

[11] Yildiz S, Amasyali MF. Iterative ensemble pseudo-labeling for convolutional neural networks. Sigma J Eng Nat Sci 2024;42:862–874. [CrossRef]

[12] Samiullah M, Ali H, Zahoor S, Ali A. Fault diagnosis on induction motor using machine learning and signal processing. arXiv preprint arXiv:2401.15417. 2024.

[13] Yutong G, Khishe M, Mohammadi M, Rashidi S, Nateri MS. Evolving deep convolutional neural networks by extreme learning machine and fuzzy slime mould optimizer for real-time sonar image recognition. Int J Fuzzy Syst 2022;24:1371–1389. [CrossRef]

[14] Hernandez-Ramirez V, Almanza-Ojeda D-L, Cardenas-Cornejo J-J, Contreras-Hernandez J-L, Ibarra-Manzano M-A. Detection of broken bars in induction motors using histogram analysis of current signals. Appl Sci 2023;13:8344. [CrossRef]

[15] Maouche Y, Oumaamar MEK, Boucherma M, Khezzar A. Instantaneous power spectrum analysis for broken bar fault detection in inverter-fed six-phase squirrel cage induction motor. Int J Electr Power Energy Syst 2014;62:110–117. [CrossRef]

[16] Agah GR, Rahideh A, Khodadadzadeh H, Khoshnazar SM, Kia SH. Broken rotor bar and rotor eccentricity fault detection in induction motors using a combination of discrete wavelet transform and Teager–Kaiser energy operator. IEEE Trans Energy Convers 2022;37:2199–2206. [CrossRef]

[17] Ameid T, Talhaoui H, Harzelli I. Broken rotor bar fault diagnosis using fast Fourier transform applied to field-oriented control induction machine: simulation and experimental study. Int J Adv Manuf Technol 2017;92:917–928. [CrossRef]

[18] Lizarraga-Morales E, Rodriguez-Donate C, Cabal-Yepez E, Ramirez ML. Novel FPGA-based methodology for early broken rotor bar detection and classification through homogeneity estimation. IEEE Trans Instrum Meas 2017;66:1760–1769. [CrossRef]

[19] Chisedzi LP, Muteba M. Detection of broken rotor bars in cage induction motors using machine learning methods. Sensors 2023;23:9079. [CrossRef]

[20] Rayyam M, Zazi M. A novel metaheuristic model-based approach for accurate online broken bar fault diagnosis in induction motor using unscented Kalman filter and ant lion optimizer. Trans Inst Meas Control 2020;42:1537–1546. [CrossRef]

[21] Ullah N, Abbas MF, Kazmi SAA, Numan M. Machine learning-based fault classification using stray flux and stator current in induction motor. In: 3rd IEEE International Conference on Artificial Intelligence (ICAI). IEEE; 2023. [CrossRef]

[22] Lee CY, Hsieh YJ, Le TA. Induction motor fault classification based on combined genetic algorithm with symmetrical uncertainty method for feature selection task. Mathematics 2020;10:230. [CrossRef]

[23] Shu Y. DBF-CNN: A double-branch fusion residual CNN for diagnosis of induction motor broken rotor bar. IEEE Trans Instrum Meas 2023;72:1–10. [CrossRef]

[24] Barrera-Llanga K, Burriel-Valencia J, Sapena-Bañó Á, Martínez-Román J. A Comparative Analysis of Deep Learning Convolutional Neural Network Architectures for Fault Diagnosis of Broken Rotor Bars in Induction Motors. Sensors (Basel) 2023;23:8196. [CrossRef]

[25] Shao S, McAleer S, Baldi P. Highly accurate machine fault diagnosis using deep transfer learning. IEEE Trans Ind Inform 2018;15:2446–2455. [CrossRef]

[26] Huang X, Xie T, Wu J, Zhou Q, Hu J. Deep continuous convolutional networks for fault diagnosis. Knowl Based Syst 2024;292:111623. [CrossRef]

[27] Khan AS, Ahmad Z, Abdullah J, Ahmad F. A spectrogram image-based network anomaly detection system using deep convolutional neural network. IEEE Access 2021;9:87079–87093. [CrossRef]

[28] Simonyan K, Zisserman A. Very deep convolutional networks for large-scale image recognition. arXiv preprint arXiv:1409.1556. 2014.

[29] Huang G, Liu Z, van der Maaten L. Densely connected convolutional networks. In: Proceedings of the IEEE Conference on Computer Vision and Pattern Recognition. IEEE; 2017. p. 4700–4708. [CrossRef]

[30] Iandola FN, Han S, Moskewicz MW, Ashraf K, Dally WJ, Keutzer K. SqueezeNet: AlexNet-level accuracy with 50× fewer parameters and <0.5 MB model size. arXiv preprint arXiv:1602.07360. 2016.

[31] He K, Zhang X, Ren S, Sun J. Deep residual learning for image recognition. In: Proceedings of the IEEE Conference on Computer Vision and Pattern Recognition. IEEE; 2016. p. 770–778. [CrossRef]

[32] Sandler M, Howard A, Zhu M, Zhmoginov A, Chen L-C. Inverted residuals and linear bottlenecks: mobile networks for classification, detection and segmentation. arXiv preprint arXiv:1801.04381. 2018. [CrossRef]

[33] Krizhevsky A, Sutskever I, Hinton GE. ImageNet classification with deep convolutional neural networks. Commun ACM 2017;60:84–93. [CrossRef]

[34] Szegedy C, Vanhoucke V, Ioffe S, Shlens J, Wojna Z. Rethinking the inception architecture for computer vision. In: Proceedings of the IEEE Conference on Computer Vision and Pattern Recognition. IEEE; 2016. p. 2818–2826. [CrossRef]

[35] Zoph B, Vasudevan V, Shlens J, Le QV. Learning transferable architectures for scalable image recognition. In: Proceedings of the IEEE Conference on Computer Vision and Pattern Recognition. IEEE; 2018. p.8697–8710. [CrossRef]

[36] Redmon J. You only look once: unified, real-time object detection. In: Proceedings of the IEEE Conference on Computer Vision and Pattern Recognition. IEEE; 2016. [CrossRef]

[37] Szegedy C, Ioffe S, Vanhocuke V, Alemi A. Inception-v4, inception-resnet and the impact of residual connections on learning. Proc AAAI Conf Artif Intell 2017;31. [CrossRef]

[38] Breiman L. Random forests. Mach Learn 2001;45:5–32. [CrossRef]

[39] Pal M. Random forest classifier for remote sensing classification. Int J Remote Sens 2005;26:217–222. [CrossRef]

[40] Watts JD, Powell S, Lawrence RL, Hilker T. Improved classification of conservation tillage adoption using high temporal and synthetic satellite imagery. Remote Sens Environ 2011;115:66–75. [CrossRef]

[41] Choubey H, Pandey A. A combination of statistical parameters for the detection of epilepsy and EEG classification using ANN and KNN classifier. Signal Image Video Process 2021;15:475–483. [CrossRef]

[42] Treml AE, Flauzino RA, Suetake M, Ravazzoli Maciejewski NA. Experimental database for detecting and diagnosing rotor broken bar in a three-phase induction motor. IEEE DataPort 2020. Available at: https://ieee-dataport.org/open-access/experimental-database-detecting-and-diagnosing-rotor-broken-bar-three-phase-induction Accessed on Sep 02, 2025.

[43] Dişli F, Gedikpınar M, Sengur A. Deep transfer learning-based broken rotor fault diagnosis for induction motors. Turk J Sci Technol 2023;18:275–290. [CrossRef]

[44] Misra S, Kumar S, Sayyad S, Bongale A, Jadhav P, Kotecha K, et al. Fault detection in induction motor using time domain and spectral imaging-based transfer learning approach on vibration data. Sensors 2022;22:8210. [CrossRef]

[45] Gundewar S, Kane P, Andhare A. Detection of broken rotor bar fault in an induction motor using convolutional neural network. J Adv Mech Des Syst Manuf 2022;16:JAMDSM0020. [CrossRef]